6184 *Biochemistry* **2009,** *48,* 6184–6190
DOI: 10.1021/bi900552c

BIOCHEMISTRY
including biophysical chemistry & molecular biology
Article

Crystal Structure and Metal Binding Properties of the Lipoprotein MtsA, Responsible for Iron Transport in *Streptococcus pyogenes*[†,‡]

Xuesong Sun,[§,@] Heather M. Baker,[∥,@] Ruiguang Ge,[⊥] Hongzhe Sun,[⊥] Qing-Yu He,*[,§] and Edward N. Baker*[,∥]

[§]*Institute of Life and Health Engineering and National Research Center of Genetic Medicine, Jinan University, Guangzhou 510632, P. R. China,* [∥]*Maurice Wilkins Centre and School of Biological Sciences, University of Auckland, Private Bag 92019, Auckland, New Zealand, and* [⊥]*Department of Chemistry, The University of Hong Kong, Pokfulam, Hong Kong* [@]*These authors contributed equally to this work*

Received April 1, 2009; Revised Manuscript Received May 22, 2009

ABSTRACT: An ability to acquire iron is essential for the viability and growth of almost all organisms and in pathogenic bacteria is strongly correlated with virulence. The cell surface lipoprotein MtsA, a component of the MtsABC transporter of *Streptococcus pyogenes*, acts as the primary receptor for inorganic iron by this significant human pathogen. Iron is bound as Fe^{2+}, with the participation of bicarbonate. The crystal structure of MtsA has been determined and refined at 1.8 Å resolution ($R = 0.167$, and $R_{free} = 0.194$). MtsA has the classic bacterial metal binding receptor (MBR) fold, with the Fe^{2+} ion bound to the side chains of His68, His140, Glu206, and Asp281, at a totally enclosed site between the two domains of the protein. The absence of bicarbonate from the binding site suggests that it is displaced during the final stages of metal binding. Both the fold and metal binding site are most similar to those of the manganese receptors PsaA and MntC, consistent with the similar coordination requirements of Fe^{2+} and Mn^{2+}. Binding studies confirm a 10-fold preference for Fe^{2+} over Mn^{2+}, although both may be carried in vivo. Mutational analysis of the binding site shows that His140 is critical for a fully functional binding site but that Glu206 is dispensable. The crystal structure explains the distinct roles of these ligands and also reveals potential secondary binding sites that may explain the binding behavior of MtsA for metal ions other than Fe^{2+}.

Iron is essential for the growth of almost all organisms because of the requirement for iron as a cofactor in many important proteins that mediate processes as diverse as oxygen and electron transport, energy production, and DNA synthesis. For pathogenic organisms, iron is therefore an important determinant of survival and virulence (*1*, *2*). To overcome the limited availability of free iron in the host environment, due to its insolubility in the presence of oxygen and its potential sequestration by host proteins, bacterial pathogens have developed a variety of mechanisms for iron acquisition (*3*). Whereas some organisms synthesize specialized iron chelators known as siderophores, others produce membrane-spanning ATP-binding cassette (ABC)[1] transporters (*4*) to scavenge iron from their microenvironments, in the form of free ferric/ferrous ions, chelated iron, or heme. Since these iron acquisition systems are surface-exposed and required for bacterial growth in the host, they are potential drug targets and vaccine candidates.

In contrast to the abundant information about the iron uptake mechanisms in Gram-negative bacteria (*5*), there is much more limited knowledge of the mechanisms for iron acquisition in Gram-positive bacteria. *Streptococcus pyogenes*, also known as Group A *Streptococcus* (GAS), is a Gram-positive human pathogen that causes a variety of human diseases, including pharyngitis, scarlet fever, necrotizing fasciitis, and streptococcal toxic shock (*6*). This organism has systems that can mediate the uptake of iron in several forms, as inorganic iron, heme, or chelated iron (*7*). MtsABC, a typical ABC transporter comprising a lipoprotein MtsA, an ATP-binding protein MtsB, and a hydrophobic integral membrane protein MtsC, provides the machinery for the uptake of inorganic iron in *S. pyogenes* (*8*, *9*). MtsA, which is anchored to the cell membrane via a lipid moiety covalently attached to its N-terminal cysteine (*10*), functions as a metal ion chelator and transporter. With the ATP-binding protein providing energy, MtsA then interacts with the integral membrane component, leading to iron release and subsequent transmembrane uptake (*8*, *10*).

[†]This work was supported by funding from the Health Research Council of New Zealand (to E.N.B.), the Chang-Jiang Scholars Program 2007, "211" Projects, and China National Science Foundation Grant 20871057 (to Q.-Y.H.), and Research Council Grants HKU722702 M and HKU751205 M (to Q.-Y.H. and H.S.).

[‡]Atomic coordinates and structure factor amplitudes have been deposited in the Protein Data Bank (entry 3hh8).

*To whom correspondence should be addressed. E.N.B.: telephone: +64-9-3737599; fax: +64-9-3737619; e-mail: ted.baker@auckland.ac.nz. Q.-Y.H.: telephone and fax: +86-20-85227039; e-mail: tqyhe@jnu.edu.cn.

[1]Abbreviations: WT, wild type; ABC, ATP-binding cassette; PBP, periplasmic binding protein; MBR, metal binding receptor; GST, glutathione *S*-transferase; PCR, polymerase chain reaction; EGTA, ethylene glycol bis(2-aminoethyl ether)-*N*,*N*,*N*′,*N*′-tetraacetic acid; GAS, Group A *Streptococcus*; ICP-MS, inductively coupled plasma mass spectroscopy; IPTG, isopropyl β-D-thiogalactopyranoside.

 Published on Web 05/22/2009

In recent years, MtsA has been cloned, expressed, and characterized (*7*−*9*, *11*). Its amino acid sequence shows that it belongs to a large family of bacterial metal binding receptor (MBR) proteins (*12*). Its closest relative for which structural data are available is the manganese receptor PsaA from *Streptococcus pneumoniae* (*13*), with which it shares ~80% sequence identity. Divergent results regarding the metal specificity of MtsA have, however, been reported from cellular studies in different laboratories (*7*−*9*). We recently showed that MtsA primarily binds ferrous ion, with bicarbonate as a synergistic anion, under relevant physiological conditions (*11*), consistent with the fact that MtsA is regulated in response to iron levels (*7*, *14*). Apart from these results, however, little is known about the detailed relationship between the structure and function of MtsA.

Here we report the crystal structure of the Fe^{2+}-bound form of MtsA (Fe-MtsA) at 1.8 Å resolution, enabling this protein to be placed in the context of the wider MBR family. The observed specificity for Fe^{2+} is explained by the nature of the ligands in the primary coordination sphere. The preparation of mutant versions of MtsA, in which the metal-binding ligands were systematically changed, coupled with studies of iron and manganese binding and iron release, has also allowed the respective roles of these ligands in structure and function to be determined.

MATERIALS AND METHODS

Materials. Chemicals used were of the highest available commercial quality. Stock solutions of HEPES, Tris-HCl, and other buffers were prepared by dissolving the respective anhydrous salts in Milli-Q water (Millipore) and adjusting the pH to the desired values with 1 M NaOH or 1 M HCl. Freshly prepared solutions of $Fe(NH_4)_2(SO_4)_2$ were used as the source of Fe^{2+}. One-kilodalton mini dialysis kits, Factor Xa, ampicillin, and isopropyl β-D-thiogalactopyranoside (IPTG) were obtained from Amersham. *Escherichia coli* BL21(DE3) star competent cells were purchased from Invitrogen. GST-binding resins were supplied by Novagen. Centricon-10 and -30 microconcentrators were obtained from Millipore. Other chemicals not specified were purchased from Sigma-Aldrich.

Protein Expression and Purification. Wild-type (WT) MtsA was expressed and purified as previously described (*11*). H68A, H140A, E206A, and D281A mutations were individually introduced into MtsA using the PCR-based QuikChange mutagenesis kit (Stratagene), with the MtsA-GST plasmid as a template. To further study the collective contribution of H68, H140, E206, and D281 to the metal binding ability of MtsA, the tetrapoint mutation H68A/H140A/E206A/D281A was produced by mutating these four amino acids to alanine. The mutated plasmids were confirmed by sequencing (TechDragon, HK) and transformed into *E. coli* BL21(DE3) star competent cells. Expression and purification of the five MtsA mutants followed the same general protocol as for the WT protein (*11*).

Equilibrium Dialysis and ICP-MS. Binding of Fe^{2+} and Mn^{2+} to WT and mutant MtsA was assessed using equilibrium dialysis and ICP-MS, as previously described (*11*). Purified proteins (200 μL at a concentration of 1 μM) were dialyzed overnight at 4 °C in 1 kDa dialysis tubing against solutions containing various concentrations of Fe^{2+} or Mn^{2+}, from 0 to 150 μM. These solutions were made up with either $Fe(NH_4)_2(SO_4)_2$ or $MnCl_2$ in 1.0 L of 50 mM HEPES and 10 μM $NaHCO_3$ (pH 7.4). Buffers were degassed for 20 min with constant mixing before the experiments and sealed with parafilm. The concentrations of metal ions were determined by ICP-MS following centrifugation at 12000*g* for 20 min to remove any possible insoluble species. The data were subjected to Hill analysis for the determination of the stoichiometry and binding affinity.

Kinetics of Release of Fe^{2+} from WT-MtsA and Mutants. The removal of Fe^{2+} from WT and mutant proteins [~25 μM in 50 mM HEPES (pH 7.4)] was monitored by UV−visible spectroscopy, based on the electronic spectral measurements previously reported (*11*). The change in absorbance at 365 nm was measured against a reference containing only the buffer and chelator (EGTA). Release constants were obtained by fitting the absorbance-versus-time data to a single-exponential function with Origin 7.1, giving R^2 values (coefficients of determination) of > 0.98 in every case (*15*).

Crystallization and Data Collection. Crystallization trials were conducted in sitting drops (100 nL of protein and 100 nL of precipitant) using a Cartesian HONEYBEE nanoliter dispensing robot (Genomic Solutions) and an in-house 480-condition crystallization screen (*16*). After optimization, the best crystals of Fe-MtsA grew at 18 °C in sitting drops comprising 2 μL of protein solution [12.0 mg/mL in 50 mM HEPES-KOH (pH 7.4), 10 mM $NaHCO_3$, and 150 mM NaCl] and 1 μL of reservoir solution [27−28% PEG MME 2K, 0.1 M $MgCl_2$, and 10 mM HEPES-KOH (pH 7.4)]. Thin, platelike, pale yellow crystals grew after 5−7 days. Crystals were flash-frozen for data collection after immersion in a cryoprotectant solution corresponding to the reservoir conditions supplemented with 22% (v/v) glycerol.

X-ray diffraction data were collected at 100 K on beamline 9-1 at the Stanford Synchrotron Radiation Laboratory (Menlo Park, CA). A complete data set was collected to 1.8 Å resolution and processed with MOSFLM and SCALA from the CCP4 program suite (*17*). The crystals were orthorhombic, in space group $P2_12_12_1$, with a Matthews coefficient of 1.99 $Å^3$/Da (38% solvent) and the following unit cell dimensions: a = 38.26 Å, b = 50.08 Å, and c = 157.62 Å. Data collection and processing statistics are listed in Table 1.

Structure Determination. Phases for the Fe-MtsA structure were determined by molecular replacement using PHASER (*18*). An ensemble of homologous structures comprising *Synechocystis* 6803 ZnuA (*19*) (PDB entry 1pq4), *Treponema pallidum* TroA (*20*) (PDB entry 1toa), and *S. pneumoniae* PsaA (*13*) (PDB entry 1psz) was used as a search model. This was followed by iterative cycles of refinement with REFMAC (*21*), incorporating translation/libration/screw (TLS) refinement (*22*) interleaved with rounds of model building using COOT (*23*). The conformation of the metal ligands and the site of the metal ion were checked at several times during the refinement, with omit maps, and found to have excellent electron density. Water molecules were added automatically and then manually checked. Only those that had good spherical electron density, reasonable B factors, and favorable hydrogen bonding contacts were retained in the model. The quality of the model was checked periodically with MOLPROBITY (*24*). Final refinement statistics are listed in Table 1.

RESULTS

Overall Structure of MtsA. The current model of MtsA consists of 280 amino acids (residues 31−310), one Fe^{2+} ion, and 268 water molecules. The protein fold (Figure 1) has the classic two-domain organization found for the wider superfamily of bacterial periplasmic binding proteins (PBPs) and other solute

Table 1: Data Collection and Refinement Details

Data Collection	
resolution range[a] (Å)	52.49−1.86 (1.96−1.86)
data collection temperature (K)	110
space group	$P2_12_12_1$
unit cell parameters	a = 38.26 Å, b = 50.08 Å, c = 157.62 Å, $\alpha = \beta = \gamma = 90.0°$
no. of unique reflections[a]	25995 (3208)
completeness[a] (%)	96.1 (86.0)
multiplicity[a]	3.9 (3.8)
R_{merge}[a] (%)	6.5 (32.0)
I/σ_I[a]	14.8 (3.5)
Refinement	
resolution range (Å)	39.41−1.87
R/R_{free}	0.167/0.194
mean B value (Å^2)	
protein atoms	2202 (13.2)
water molecules	268 (22.7)
ligand atoms	1 Fe (9.8)
root-mean-square deviations from standard values	
bond lengths (Å)	0.016
bond angles (deg)	1.54
Ramachandran plot	
% residues in favored regions	97.1
outliers	−

[a] Figures in parentheses are for the outermost resolution shell.

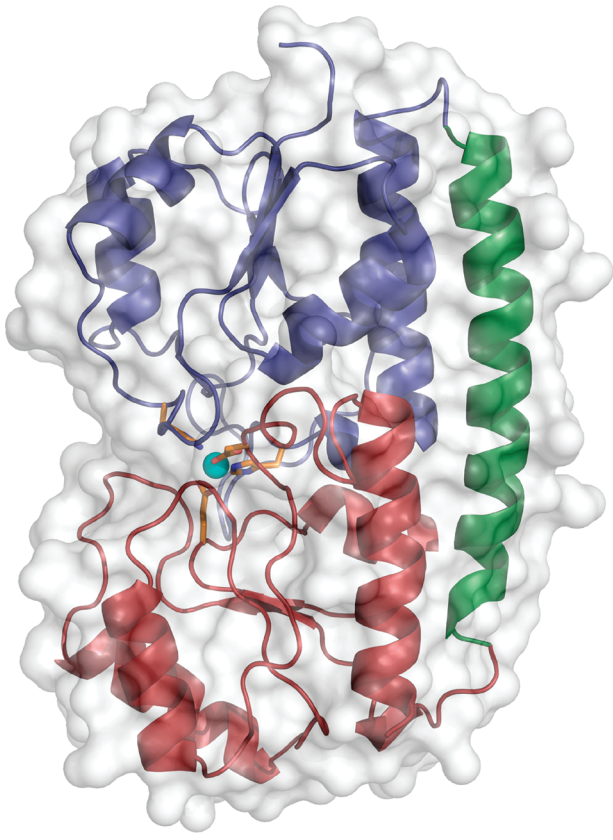

FIGURE 1: Structure of MtsA. The fold of the protein is shown as a ribbon diagram, inside a transparent molecular surface. The N-terminal domain (blue) is at the top of the view, the C-terminal domain (red) at the bottom, and the slightly curved backbone α-helix (green) at the right. The location of the iron site is shown with a cyan sphere, representing the bound Fe^{2+} ion, surrounded by the four ligands, in stick representation.

binding receptors (*25*), but with a specific topology that is characteristic of the metal binding receptor (MBR) family (*12*). The most striking feature of this fold is a long α-helix [residues 164−190, helix d′ in the terminology used for PsaA (*13*)] that runs the full length of the molecule, providing the only link between the N- and C-terminal domains (*13*, *20*). This helix gives a relatively rigid backbone to the structure but is slightly curved, subtending an angle of ~10°. Two $(\alpha/\beta)_4$ domains, each comprising a four-stranded β-sheet with helices packed on either face, pack against this helix and face each other across a large interface which provides the ligands for the metal binding site.

The two domains can be superimposed with a root-mean-square (rms) difference in atomic positions of 3.0 Å for 89 of 116 Cα atoms in spite of having a sequence identity of only 11%. This gives a pseudosymmetric character to the domain interface. The metal binding site is ~6 Å from one end of the interface and ~20 Å from the backbone helix d′ at the other end of the interface (Figure 1). Between the metal binding site and helix d′ is a large buried surface comprising 1170 Å^2 of the N-domain (15% of its total surface) and 1229 Å^2 of the C-domain (18% of its surface). This buried surface includes 13 hydrogen bonds and one salt bridge that are formed across the interface.

The helical backbone in MtsA and other MBRs raises the question of how bound metal ions or other ligands are released. There is no evidence for large hinge-bending conformational changes like those that occur for the PBPs (*26*). Rather, the position of the metal binding site so close to the outer end of the interface suggests that only limited movement is needed to effect metal ion release (*20*, *26*). This could occur by straightening of the backbone helix, such as is seen for the B_{12}-binding protein BtuF (*27*), in which this helix is straight and the two domains are farther apart, to accommodate the larger B_{12} molecule. Alternatively, movement of some of the metal ligands may be sufficient, as is seen in a metal-free variant of ZnuA (*28*).

Comparison with Other MBR Proteins. Searches of the Protein Data Bank using SSM (*29*) show that the closest structural homologues of MtsA are the two manganese receptor proteins, PsaA from *S. pneumoniae* (*13*) and MntC from *Synechocystis* 6803 (*30*). These align very closely with MtsA: for PsaA, the rms difference is only 0.64 Å for 277 Cα atom positions (97% of the modeled structure), and for MntC, the rms difference is 1.24 Å for 266 Cα atoms. The next closest homologue (rms difference of 1.43 Å for 262 Cα atoms) is TroA from *Treponema pallidum* (*20*), which has specificity for both manganese and zinc, followed by zinc receptors such as ZnuA (*19*, *31*, *32*) and AdcAII (*33*) with rms differences of ~2.0 Å. These structural relationships nicely fit with sequence-based phylogenetic analyses (*12*, *33*), which have enabled the MBRs to be subdivided into subfamilies that are specific either for iron and manganese or for zinc.

Iron Binding Site. The iron binding site of MtsA is located ~6 Å below the molecular surface, between the two domains (Figure 1). The four iron ligands comprise two histidines and two carboxylates and are contributed by both domains, and different structural elements within them. The two histidine ligands, His68 and His140, are contributed by the N-terminal domain, with His68 close to the opening of the binding cleft, where its Nδ1 atom is exposed to solvent, and His140 deeply buried at the back. The two carboxylate ligands, Glu206 and Asp281, are both contributed by the C-terminal domain and also differ in their exposure, with Glu206 closer to the opening of the cleft and

Asp281 more buried. It is significant that the two ligands that move in the zinc-free form of ZnuA (*28*) are the outermost ligands, corresponding to His68 and Glu206 in MtsA. Although the metal ion is bound to only these protein ligands, this part of the interface is not tightly packed and contains a number of solvent molecules that occupy small cavities.

The Fe^{2+} ion is coordinated through four strong bonds and two weaker interactions (Table 2), generating a highly distorted octahedral site in which both carboxylate ligands have asymmetric bidentate coordination (Figure 2). The metal ion is completely enclosed by the four ligands, leaving no coordination position available for solvent (water or bicarbonate) unless one of the protein ligands was to dissociate. The metal coordination environment is identical to that of the two manganese-binding MBRs, PsaA and MntC (*13*, *30*). The metal binding sites for both of the latter proteins have some uncertainty, however; for PsaA, this concerns the identity of the bound metal (Mn or Zn), whereas for MntC, the resolution of the structure was only moderate (2.9 Å). The metal ion bound in our MtsA structure is assumed to be Fe^{2+}, from its mode of preparation and color, although it is possible that some oxidation to Fe^{3+} takes place during crystallization, since the binding site will accept both, albeit with a 3-fold preference for Fe^{2+} over Fe^{3+} (*11*). In any case, the metal binding mode seen here serves as a model for the subfamily of iron- and manganese-specific MBRs, which all share two His and two Glu/Asp ligands, in contrast to the zinc-specific MBRs which have three His ligands and one Glu/Asp (*12*, *33*).

Table 2: Metal−Ligand Bond Distances and Associated Hydrogen Bond Distances

atom	atom	distance (Å)
Fe	His68 Nε2	2.08
Fe	His140 Nε2	2.02
Fe	Glu206 Oε1	2.08
Fe	Glu206 Oε2	2.44
Fe	Asp281 Oδ2	1.97
Fe	Asp281 Oδ1	2.80
	Hydrogen Bonds	
His68 Nδ1	HOH 3 O	2.80
His140 Nδ1	Asp138 Oδ2	2.81
Glu206 Oε2	Asn227 N	2.93
Asp281 Oδ2	HOH 113 O	2.72
Glu206 Oε1	HOH 112 O	2.83
Asn227 Nδ2	HOH 113 O	3.07
Glu255 Oε2	HOH 112 O	2.79
Ser257 Oγ	HOH 113 O	2.71
HOH 112 O	HOH 113 O	2.82

Mutational Analysis of Binding and Release. The individual and collective importance of the four iron-binding ligands was tested by mutagenesis. The resulting four single-point mutant proteins, H68A, H140A, E206A, and D281A, and one tetrapoint mutant, H68A/H140A/E206A/D281A, were expressed and purified with procedures similar to those used for WT-MtsA (*11*).

Binding constants for binding of both Fe^{2+} and Mn^{2+} to the mutant MtsAs were determined by equilibrium dialysis and ICP-MS (Figures S1 and S2 of the Supporting Information). These data showed that both WT-MtsA and the E206A mutant had

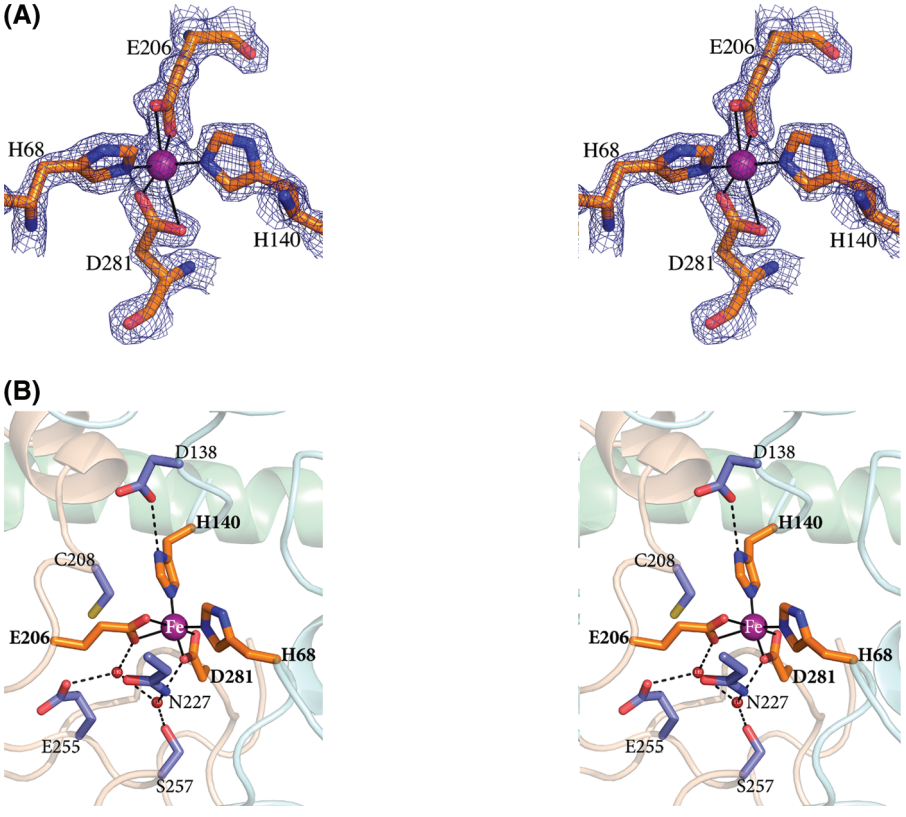

FIGURE 2: Iron binding site, shown in stereo. (A) Electron density from a $2F_o - F_c$ map, contoured at 2.0σ. The Fe^{2+} ion is shown as a magenta sphere, bonded to its four protein ligands (orange, with atom coloring, drawn in stick representation). The covalent metal−ligand bonds are shown as thin lines. (B) Wider environment of the iron binding site. Second-shell residues are colored blue (stick mode, with atom coloring). Below the iron site is the possible secondary metal binding site, filled in the crystal structure by two water molecules (red spheres). Hydrogen bonds are shown as dashed lines. Key distances are given in Table 2.

Table 3: Binding Constants for Fe^{2+} and Mn^{2+} and Rate Constants for Iron Release from WT and Mutant Proteins

	K (M^{-1}) (for Fe^{2+} binding)	K (M^{-1}) (for Mn^{2+} binding)	k (min^{-1})
WT-MtsA	$(2.32 \pm 0.15) \times 10^5$	$(2.01 \pm 0.17) \times 10^4$	0.005 ± 0.000
H68A	$(5.18 \pm 0.32) \times 10^3$	$(5.92 \pm 0.22) \times 10^3$	0.192 ± 0.006
H140A	$(3.75 \pm 0.18) \times 10^3$	$(4.90 \pm 0.23) \times 10^3$	0.610 ± 0.039
E206A	$(1.52 \pm 0.18) \times 10^5$	$(1.35 \pm 0.21) \times 10^4$	0.014 ± 0.001
D281A	$(1.31 \pm 0.34) \times 10^4$	$(1.28 \pm 0.24) \times 10^4$	0.101 ± 0.002
tetra mutant	$(2.25 \pm 0.19) \times 10^3$	$(3.86 \pm 0.26) \times 10^3$	0.826 ± 0.019

approximately 1:1 stoichiometry with Fe^{2+} and that the affinity of E206A for Fe^{2+} was only slightly reduced (1.5-fold). The other mutants had much lower stoichiometries, with affinities reduced 18-fold for D281A, 46-fold for H68A, 60-fold for H140A, and more than 100-fold for the tetra mutant (Table 3). Even the tetra mutant exhibited some residual binding (~0.3 mol), presumably nonspecific. Similar patterns were seen for Mn^{2+} binding (Table 3). WT-MtsA binds Mn^{2+} 10-fold more weakly than Fe^{2+}. The reduction in binding affinity of the mutants was much less pronounced than for Fe^{2+}, ranging from 1.5-fold for E206A and D281A to 5-fold for the tetra mutant, reflecting a higher contribution from nonspecific binding.

Measurement of iron release kinetics, using a competition assay between MtsA and EGTA, showed an exponential decrease in the absorbance at 365 nm with a half-time of ca. 130 min, indicative of a gradual release of iron from MtsA (Figure S3 of the Supporting Information). A pseudo-first-order kinetics equation gave a satisfactory fit to the curve and an iron release rate constant k of 0.005 min^{-1}. The release rate increased when more EGTA was added to the reaction solution, and the rate constants with respect to EGTA concentration could be appropriately fitted to a Hill plot (Figure S3 of the Supporting Information), indicating that release of iron from WT-MtsA followed a saturation mode of kinetics. Similar kinetics were shown by the mutant proteins (Table 3). Iron release rates were found to increase in the following order: WT-MtsA (0.005 min^{-1}) < E206A (0.014 min^{-1}) ≪ D281A (0.101 min^{-1}) < H68A (0.192 min^{-1}) < H140A (0.610 min^{-1}) < tetra mutant (0.826 min^{-1}), reciprocally consistent with the Fe^{2+} binding affinities.

DISCUSSION

The MtsA protein has superficial structural similarities with the eukaryotic iron-binding proteins, transferrin and lactoferrin (*34*), and their bacterial analogues, the periplasmic iron-binding proteins of Gram-negative bacteria (*35*−*37*). All of these proteins share the property that the metal ion is bound between two domains, to ligands that are contributed from both domains. This means that relative domain movements can be coupled to metal ion release.

There are significant differences, however, that reflect the different family to which MtsA belongs and its different physiological function. First, in MtsA, as in other members of the MBR family, the metal site is much closer to the protein surface than in the transferrins, and an α-helix spanning the two domains ensures that no large conformational change accompanies metal ion release. This contrasts with the transferrins and their bacterial analogues, in which β-strands link the two domains and allow large-scale domain movements (*36*). Second, the binding site in MtsA favors the binding of divalent metal ions, compared with the trivalent preference of the transferrins, and this is achieved by the choice of ligands: two neutral His residues and two carboxylates for MtsA (overall 2− charge) compared with one His, one carboxylate, and two tyrosinates for transferrins (*34*) (overall 3− charge). The use of tyrosine ligands in particular appears to give a high affinity for iron (typically ~10^{20} M^{-1}), as is shown for both the transferrins and their bacterial analogues. This is consistent also with the use of catecholate ligands in many bacterial siderophores (*38*). In contrast, metal ion affinities are lower in the MBRs, they have less specific ligand sets, and they have more promiscuous metal binding roles.

The absence of bicarbonate from the Fe^{2+} coordination sphere in MtsA was unexpected, given the NMR evidence for direct coordination of the anion (*11*). The ligand movements seen in ZnuA (*28*), however, suggest that the two outer ligands, His68 and Glu206, may be similarly "flipped" out in the metal-free form of MtsA. Bicarbonate may then be bound to the Fe^{2+} ion in the initial stages of binding, to be replaced by Glu206 as closure around the metal ion is completed. The failure of ions such as citrate to fill the same role may be explained by the relatively low affinity of MtsA for Fe^{2+}, since stronger chelating ions might not be displaced. The specificity for Fe^{2+} over Fe^{3+} in MtsA is consistent with the presence of only two negatively charged ligands in the coordination sphere and the lack of room for solvent or coordinating anions. It contrasts with the transferrins in which Fe^{3+} is strongly preferred and carbonate is incorporated in the primary coordination sphere (*34*).

Selective mutation of each of the ligands in the primary metal binding site of MtsA clearly points to differences in their roles in the binding site. Mutations of three of the ligands, His68, His140, and Asp281, in each case substantially decreased Fe^{2+} binding affinities and dramatically accelerated the release of iron from the mutant proteins. On the other hand, elimination of the fourth ligand, Glu206, had only minor effects on iron binding and release (Table 2). In addition, ICP-MS measurements revealed that the E206A mutant protein binds iron stably with ~1:1 stoichiometry, similar to that of WT-MtsA. This suggests that Glu206 may not be essential for iron binding in MtsA. This ligand could be replaced by bicarbonate in the E206A protein, since the binding assays were conducted in 10 μM $NaHCO_3$, or by other buffer ions. Alternatively, an adjacent residue, Asn227, could substitute for it in the coordination sphere (Figure 2). By taking a different rotamer, this residue can extend its Oδ1 atom to within 2.8 Å of the Fe^{2+} ion. A concomitant small movement of the metal ion would enable stable binding.

Of the other ligands, mutation of His140 has the most dramatic effect on iron binding; apart from the tetra mutant, the H140A has the lowest iron binding constant, the fastest iron release rate, and the lowest iron content in ICP-MS determination. This can be explained by the fact that His140 is the most deeply buried ligand and makes a strong hydrogen bond with Asp138 Oδ1 (Figure 2). It thus contributes not only to iron coordination but also to the stability and spatial organization of

the whole binding site. His140 is fully conserved in all MBR sequences, and we conclude, as may be also inferred from studies with ZnuA (*28*), that this ligand acts as an anchor for the metal binding site.

Intriguingly, the tetra mutant still held some iron binding ability. This points to the likely existence of one or more secondary metal binding sites in MtsA, such as has already been found in the zinc-binding ZnuA (*32*). Two possible sites are apparent from the MtsA structure. The first is ~4.5 Å from the primary iron-binding site, where two water molecules, OW112 and OW113, occupy a small cavity (Figure 2) bounded by Glu206 and Asp281 (both iron ligands) together with Cys208, Asn227, Glu255, and Ser257. In the absence of the primary ligands, this site would be readily accessible to a metal ion. The presence of Cys208 at this site is intriguing as it may explain the fact that MtsA binds both Zn^{2+} and Cu^{2+} in a 2:1 ratio (*11*); both these metal ions would be attracted to the "soft" sulfur ligand. Another interesting possibility is on the MtsA surface where Tyr222 is equivalent to His224 in ZnuA. The latter provides a second binding site for zinc in ZnuA (*32*), and Tyr222 could contribute to secondary iron binding by MtsA, given its affinity for Fe^{3+}. Again, buffer ions could also participate in any secondary or nonspecific binding.

The structural and functional data presented here and previously (*11*) show that the primary specificity of MtsA in vitro is for Fe^{2+}. The likely physiological role of MtsA is a more subtle question, however. As a human hemolytic pathogen causing acute inflammatory infections, *S. pyogenes* is likely to be exposed to low levels of free iron, but much higher levels of heme, released from hemoproteins. Its main source of iron may thus be through the analogous heme transporter, HtsA (*7*). Studies on the regulation of MtsA expression show that levels of MtsA are depressed by added Fe^{3+} and Mn^{2+}, but not Zn^{2+}, and that the effects are most dramatic with Mn^{2+} (*14*). This implies a role in both iron and manganese homeostasis in vivo, even though its in vitro binding ability favors iron. It is also noteworthy that although there is strong similarity in the metal binding site through all MBRs, MtsA does not seem to have an in vivo role in zinc homeostasis, which is instead controlled by another MBR member, Lsp, in *S. pyogenes* (*39*).

ACKNOWLEDGMENT

We thank Dr. Tom Caradoc-Davies for help with data collection and processing. The X-ray data were collected at the Stanford Synchrotron Radiation Laboratory (SSRL), which is funded by the Department of Energy (BES, BER) and the National Institutes of Health (NCRR, NIGMS). We thank Dr. Clyde Smith and other staff at the SSRL for assistance.

SUPPORTING INFORMATION AVAILABLE

Binding of Fe^{2+} to WT and mutant MtsAs (Figure S1), Binding of Mn^{2+} to WT and mutant MtsAs (Figure S2), and kinetics of iron release by EGTA from Fe^{2+}-saturated MtsA (Figure S3).

This material is available free of charge via the Internet at http://pubs.acs.org.

REFERENCES

(1) Weinberg, E. D. (1974) Iron and susceptibility to infectious disease. *Science 184*, 952–956.
(2) Ratledge, C., and Dover, L. G. (2000) Iron metabolism in pathogenic bacteria. *Annu. Rev. Microbiol. 54*, 881–941.
(3) Brown, J. S., and Holden, D. W. (2002) Iron acquisition by Gram-positive bacterial pathogens. *Microbes Infect. 4*, 1149–1156.
(4) Higgins, C. F. (2001) ABC transporters: Physiology, structure and mechanism—an overview. *Res. Microbiol. 152*, 205–210.
(5) Briat, J. F. (1992) Iron assimilation and storage in prokaryotes. *J. Gen. Microbiol. 138*, 2475–2483.
(6) Cunningham, M. W. (2000) Pathogenesis of Group A Streptococcal Infections. *Clin. Microbiol. Rev. 13*, 470–511.
(7) Lei, B., Liu, M., Voyich, J. M., Prater, C. I., Kala, S. V., DeLeo, F. R., and Musser, J. M. (2003) Identification and characterization of HtsA, a second heme-binding protein made by *Streptococcus pyogenes*. *Infect. Immun. 71*, 5962–5969.
(8) Janulczyk, R., Pallon, J., and Bjorck, L. (1999) Identification and characterization of a *Streptococcus pyogenes* ABC transporter with multiple specificity for metal cations. *Mol. Microbiol. 34*, 596–606.
(9) Janulczyk, R., Ricci, S., and Bjorck, L. (2003) MtsABC is important for manganese and iron transport, oxidative stress resistance, and virulence of *Streptococcus pyogenes*. *Infect. Immun. 71*, 2656–2664.
(10) Sutcliffe, I. C., and Russell, R. R. B. (1995) Lipoproteins of Gram-positive bacteria. *J. Bacteriol. 177*, 1123–1128.
(11) Sun, X., Ge, R., Chiu, J.-F., Sun, H., and He, Q.-Y. (2008) Lipoprotein MtsA of MtsABC in *Streptococcus pyogenes* primarily binds ferrous ion with bicarbonate as synergistic anion. *FEBS Lett. 582*, 1351–1354.
(12) Claverys, J.-P. (2001) A new family of high-affinity ABC manganese and zinc permeases. *Res. Microbiol. 152*, 231–243.
(13) Lawrence, M. C., Pilling, P. A., Epa, V. C., Berry, A. M., Ogunniyi, A. D., and Paton, J. C. (1998) The crystal structure of pneumococcal surface antigen PsaA reveals a metal-binding site and a novel structure for a putative ABC-type binding protein. *Structure 6*, 1553–1561.
(14) Hanks, T. S., Liu, M., McClure, M. J., Fukumura, M., Duffy, A., and Lei, B. (2006) Differential regulation of iron- and manganese-specific MtsABC and heme-specific HtsABC transporters by the metalloregulator MtsR of Group A Streptococcus. *Infect. Immun. 74*, 5132–5139.
(15) He, Q. Y., Mason, A. B., Woodworth, R. C., Tam, B. M., MacGillivray, R. T. A., Grady, J. K., and Chasteen, N. D. (1997) Inequivalence of the two tyrosine ligands in the N-lobe of human serum transferrin. *Biochemistry 36*, 14853–14860.
(16) Moreland, N., Ashton, R., Baker, H. M., Ivanovic, I., Patterson, S., Arcus, V. L., Baker, E. N., and Lott, J. S. (2005) A flexible and economical medium-throughput strategy for protein production and crystallization. *Acta Crystallogr. D61*, 1378–1385.
(17) Collaborative Computational Project No. 4 (1994) The CCP4 Suite: Programs for Protein Crystallography. *Acta Crystallogr. D50*, 760–763.
(18) Storoni, L. C., McCoy, A. J., and Read, R. J. (2004) Likelihood-enhanced fast rotation functions. *Acta Crystallogr. D60*, 432–438.
(19) Banerjee, S., Wei, B., Bhattacharyya-Pakrasi, M., Pakrasi, H. B., and Smith, T. J. (2003) Structural determinants of metal specificity in the zinc transport protein ZnuA from *Synechocystis* 6803. *J. Mol. Biol. 333*, 1061–1069.
(20) Lee, Y.-H., Deka, R. K., Norgard, M. V., Radolf, J. D., and Hasemann, C. A. (1999) *Treponema pallidum* TroA is a periplasmic zinc-binding protein with a helical backbone. *Nat. Struct. Biol. 6*, 628–633.
(21) Murshudov, G. N., Vagin, A. A., and Dodson, E. J. (1997) Refinement of macromolecular structures by the maximum-likelihood method. *Acta Crystallogr. D53*, 240–255.
(22) Winn, M., Isupov, M., and Murshudov, G. N. (2000) Use of TLS parameters to model anisotropic displacements in macromolecular refinement. *Acta Crystallogr. D57*, 122–133.
(23) Emsley, P., and Cowtan, K. (2004) Coot: Model-building tools for molecular graphics. *Acta Crystallogr. D60*, 2126–2132.
(24) Richardson, J. S., Arendall, W. B., and Richardson, D. C. (2003) New tools and data for improving structures, using all-atom contacts. *Methods Enzymol. 374*, 385–412.
(25) Tam, R., and Saier, M. H. J. (1993) Structural, functional and evolutionary relationships among extracellular solute-binding receptors of bacteria. *Microbiol. Rev. 57*, 320–346.
(26) Krewulak, K. D., Shepherd, C. M., and Vogel, H. J. (2005) Molecular dynamics simulations of the periplasmic ferric-hydroxamate binding protein FhuD. *BioMetals 18*, 375–386.
(27) Borths, E. L., Locher, K. P., Lee, A. T., and Rees, D. C. (2002) The structure of *Escherichia coli* BtuF and binding to its cognate ATP

binding cassette transporter. *Proc. Natl. Acad. Sci. U.S.A. 99*, 16642–16647.
(28) Wei, B., Randich, A. M., Bhattacharyya-Pakrasi, M., Pakrasi, H. B., and Smith, T. J. (2007) Possible regulatory role for the histidine-rich loop in the zinc transport protein, ZnuA. *Biochemistry 46*, 8734–8743.
(29) Krissinel, E., and Henrick, K. (2004) Secondary-structure matching (SSM), a new tool for fast protein structure alignment in three dimensions. *Acta Crystallogr. D60*, 2256–2268.
(30) Rukhman, V., Anati, R., Melamed-Frank, M., and Adir, N. (2005) The MntC crystal structure suggests that import of Mn^{2+} in cyanobacteria is redox controlled. *J. Mol. Biol. 348*, 961–969.
(31) Chandra, B. R., Yogavel, M., and Sharma, A. (2007) Structural analysis of ABC-family periplasmic zinc binding protein provides new insights into mechanism of ligand uptake and release. *J. Mol. Biol. 367*, 970–982.
(32) Yatsunyk, L. A., Easton, J. A., Kim, L. R., Sugarbaker, S. A., Bennett, B., Breece, R. M., Vorontsov, I. I., Tierney, D. L., Crowder, M. W., and Rosenzweig, A. L. (2008) Structure and metal binding properties of ZnuA, a periplasmic zinc transporter from *Escherichia coli*. *J. Biol. Inorg. Chem. 13*, 271–288.
(33) Loisel, E., Jacquamet, L., Serre, L., Bauvois, C., Ferrer, J. L., Vernet, T., Di Guilmi, A. M., and Durmort, C. (2008) AdcAII, a new pneomococcal Zn-binding protein homologous with ABC transporters: Biochemical and structural analysis. *J. Mol. Biol. 381*, 594–606.
(34) Baker, E. N. (1994) Structure and reactivity of transferrins. *Adv. Inorg. Chem. 41*, 389–463.
(35) Bruns, C. M., Nowalk, A. J., Arvai, A. S., McTigue, M. A., Vaughan, K. G., Mietzner, T. A., and McRee, D. E. (1997) Structure of *Haemophilus influenzae* Fe^{3+}-binding protein reveals convergent evolution within a superfamily. *Nat. Struct. Biol. 4*, 919–924.
(36) Koropatkin, N., Randich, A. M., Bhattacharyya-Pakrasi, M., Pakrasi, H. B., and Smith, T. J. (2007) The structure of the iron-binding protein, FutA1, from *Synechocystis* 6803. *J. Biol. Chem. 282*, 27468–27477.
(37) Badarau, A., Firbank, S. J., Waldron, K. J., Yanagisawa, S., Robinson, N. J., Banfield, M. J., and Dennison, C. (2008) FutA2 is a ferric binding protein from *Synechocystis* PCC 6803. *J. Biol. Chem. 283*, 12520–12527.
(38) Neilands, J. B. (1981) Microbial iron compounds. *Annu. Rev. Biochem. 50*, 715–731.
(39) Weston, B. F., Brenot, A., and Caparon, M. G. (2009) The metal homeostasis protein Lsp of *Streptococcus pyogenes* is necessary for acquisition of zinc and virulence. *Infect. Immun.* doi 10.1128/IAI.01299-08.